Alignment of 4-mirror Wide Field Corrector for the Hobby-Eberly Telescope

Chang Jin Oh*[a], Eric H. Frater[a], Laura Coyle[a], Matt Dubin[a], Andrew Lowman[a], Chunyu Zhao[a], James H. Burge[a]

[a]College of Optical Sciences, The University of Arizona,
1630 E. University Blvd, Tucson, AZ, USA 85721

ABSTRACT

The Hobby-Eberly Telescope (HET) Wide Field Corrector (WFC) is a four-mirror optical system which corrects for aberrations from the 10-m segmented spherical primary mirror. The WFC mirror alignments must meet particularly tight tolerances for the system to meet performance requirements. The system uses 1-m class highly aspheric mirrors, which precludes conventional alignment methods. For the WFC system align a "center reference fixture" has been used as the reference for each mirror's vertex and optical axis. The center reference fixtures have both a CGH and sphere mounted retroreflector (SMR) nests. The CGH is aligned to the mirror's optical axis to provide a reference for mirror decenter and tilt. The vertex of each mirror is registered to the SMR nests on the center reference fixtures using a laser tracker. The spacing between the mirror vertices is measured during the system alignment using these SMR nest locations to determine the vertex locations. In this paper the procedures and results from creating and characterizing these center reference fixtures are presented. As a verification of proposed alignment methods the results from their application in the WFC system alignment are also presented.

Keywords: Hobby-Eberly Telescope Wide Field Corrector, Aspheric Mirror, Alignment, Center Reference Fixture

1. INTRODUCTION

The Hobby-Eberly Telescope (HET) Wide Field Corrector (WFC) is a four-mirror optical system that requires a particularly challenging alignment [1]. In order to correct the aberrations introduced by the 10-m segmented spherical primary mirror this mirror system uses 1-m class highly aspheric mirrors which precludes conventional alignment techniques. The system layout is shown in Figure 1 with its optical prescription and tolerances given in Table 1 and Table 2, respectively [2].
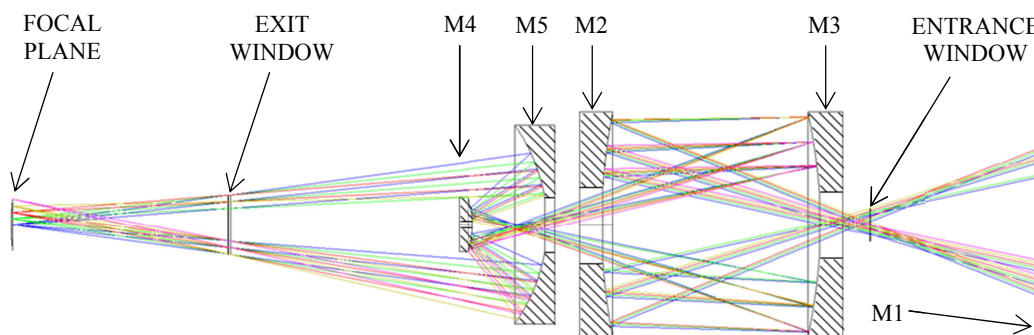
Figure 1. Hobby-Eberly Telescope wide field corrector system layout. (M1 is not shown in the figure.)

To achieve a successful alignment of the wide file corrector the center reference fixtures have been developed [3]. The center reference fixtures have a phase-etched Fresnel zone plate CGH mounted at their center which is normal to and centered on the optical axis of each mirror. During the alignment M5, M2, and M3 are individually aligned to M4 which defines the nominal optical axis. There are also SMR (sphere mounted retroreflector) nests on the center reference

* cjoh@optics.arizona.edu; Phone 520-626-5454

fixtures that are registered to the vertex of each mirror. The mirrors are aligned in spacing by using a laser tracker and SMRs to locate these nests and construct the vertex location of each mirror to determine the needed adjustment. The laser tracker is also used to place the mirrors in their nominal positions within the mounting structure to bring their positions within range for fine alignment. This paper describes the methods used to register the center reference fixtures to the optical axes and vertices of each mirror with results given to demonstrate our success. The use of these references in the system alignment is also reported to confirm the practicality of this alignment scheme for systems with multiple large aspheric mirrors.

Table 1. Hobby-Eberly Telescope optical prescription with the wide field corrector

Surface	Radius of curvature (mm)	Conic constant	Thickness (mm)
M1	-26163.900	0.0000	-14006.420
M2	2620.660	0.6635	986.890
M3	-2032.428	-7.7114	-1569.597
M4	-376.630	-2.0984	336.820
M5	-742.046	-0.2684	-2410.618
Focal plane	980.650	0.0000	-

Table 2. Wide field corrector alignment tolerances

Degree of Freedom	Tolerance	Unit
M2 to M3 axial	100	μm
M2 to M5 axial	100	μm
M4 to M5 axial	20	μm
M2 decenter (X or Y)	50	μm
M3 decenter (X or Y)	50	μm
M4 decenter (X or Y)	20	μm
M4 M5 decenter (X or Y)	50	μm
M2 tilt (X or Y)	2.808E-03	deg
M3 tilt (X or Y)	2.808E-03	deg
M4 tilt (X or Y)	4.621E-03	deg
M4 M5 tilt (X or Y)	3.183E-03	deg

2. THE CENTER REFERENCE FIXTURE

Each mirror in the wide field corrector has alignment references which are referred to as center reference fixtures. Representative examples of these fixtures are shown in Figure 2. The fixture is kinematically mounted to three V-blocks about the geometrical axis of each mirror. The center reference fixtures all have a CGH mounted at their center. This CGH is used as a reference for the decenter and tilt alignments. There are also three sphere mounted retroreflector (SMR) nests bonded to the fixtures for M2, M3, and M5. The SMR nests provide a reference for the axial location of each mirror vertex. The vertex of M4 is referenced to a single SMR on a separate fixture, also shown in Figure 2, which uses the backplane of the mirror as the datum for vertex location.
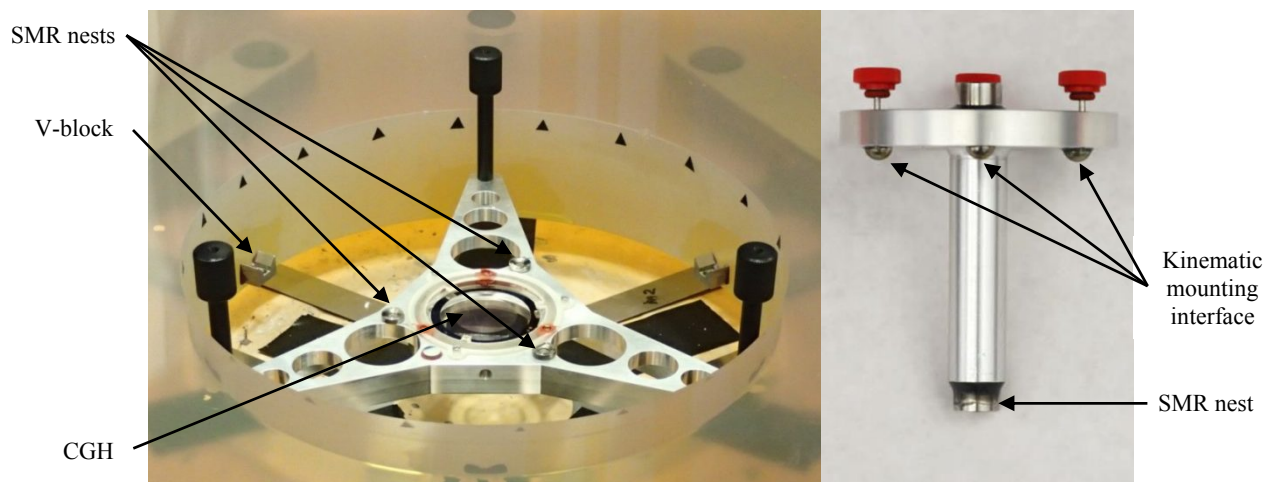
Figure 2. Photograph of the M2 center reference fixture (left) and M4 vertex fixture (right)

2.1 Registration of the optical axis to the center reference fixture

In order to align the CGH optical axis with the optical axis of the mirror the set up in the Figure 3 was used. As shown in the Figure, the set up consists of a precision air-bearing, an interferometer and CGH to evaluate the wavefront of the optical surface and a point source microscope to monitor the CGH in the center reference fixture. The general procedure to register the CGH to the optical axis of the mirror is given below.

STEP 1: Align decenter and tilt of the optical axis of the mirror relative to the axis of rotation of the air-bearing by evaluation of modulations in coma and tilt induced by misalignments.

STEP 2: Install the center reference fixture, with the CGH installed, and the point source microscope.

STEP 3: Align the optical axis of the CGH relative to the axis of rotation in decenter by evaluation of the CGH center mark coordinates on rotation.

STEP 4: Align the optical axis of the CGH relative to the axis of rotation in tilt by evaluation of the CGH angle on rotation with the point source microscope in the autocollimator mode.
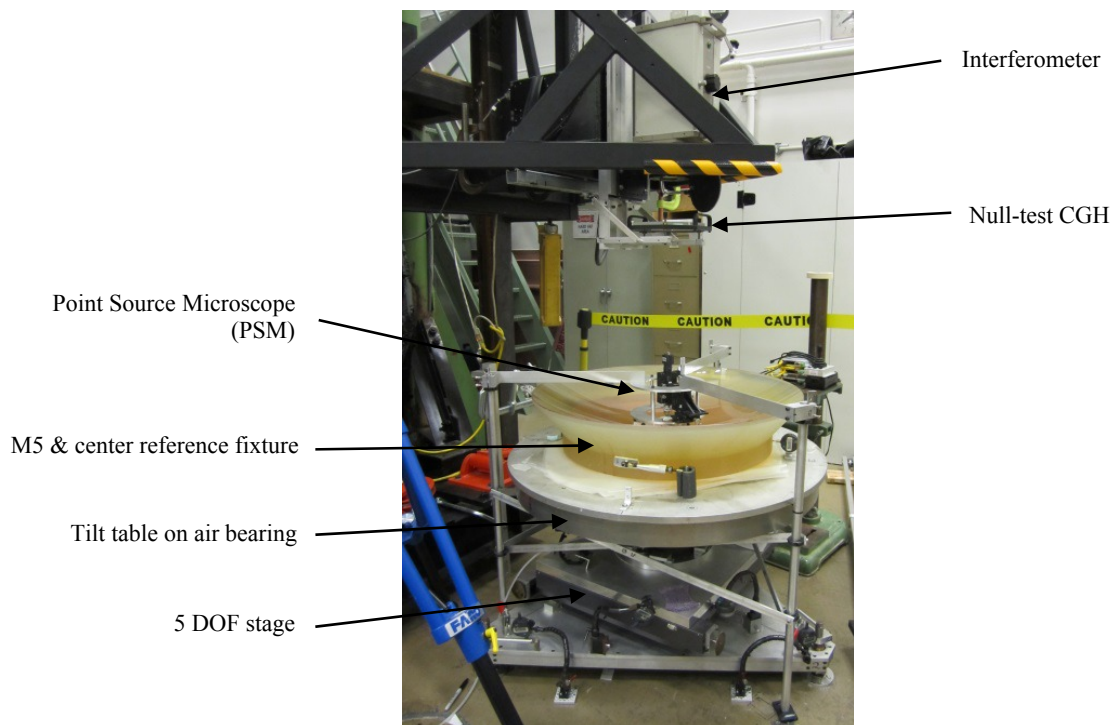
Figure 3. Center reference fixture alignment with the optical axis of M5 using null CGH test and PSM on a rotary air bearing.

2.2 Mirror alignment to axis of mirror rotation

In order to clearly explain the concepts presented in this paper, a set of labels for the relevant aberration coefficients is used. The notation for the aberration coefficients is summarized in Table 3. The labels for misalignments of the mirror or CGH are explained in Table 4.

Table 3. Zernike fringe aberration coefficient

Zernike Coefficient	Wavefront fit polynomial
Z_2	$\rho\cos\theta$
Z_3	$\rho\sin\theta$
Z_7	$(3\rho^3 - 2\rho)\cos\theta$
Z_8	$(3\rho^3 - 2\rho)\sin\theta$

Table 4. Mirror misalignment labels

Misalignment Label	Description of Mirror/CGH Position
θ_x	Sloped along x-axis, tilted about y-axis
θ_y	Sloped along y-axis, tilted about x-axis
Δ_x	Decentered along x-axis
Δ_y	Decentered along y-axis

Each aspheric mirror in the WFC has an associated null CGH test which is used to test the aspheric surface of the mirror. The null test for each mirror was simulated in Zemax in order to find the sensitivities of tilt and third-order coma Zernike coefficients to misalignments of the mirror. Simulated misalignments were introduced at the vertex of each mirror and sensitivities of the Zernike coefficients were evaluated for decenter and tilt independently. The net Zernike coefficients from a given decenter, Δ, and tilt, θ, in x and y direction are described in Equation (1) and Equation (2) respectively.

$$\begin{bmatrix} Z_2 \\ Z_7 \end{bmatrix} = \begin{bmatrix} \emptyset_{11} & \emptyset_{12} \\ \emptyset_{21} & \emptyset_{22} \end{bmatrix} \cdot \begin{bmatrix} \Delta_x \\ \theta_x \end{bmatrix} \quad (1)$$

where the sensitivity is defined as,

$$\emptyset_{11} = Z_{2\Delta}/\Delta_x, \ \emptyset_{12} = Z_{2\theta}/\theta_x, \ \emptyset_{21} = Z_{7\Delta}/\Delta_x \text{ and } \emptyset_{22} = Z_{7\theta}/\theta_x.$$

$$\begin{bmatrix} Z_3 \\ Z_8 \end{bmatrix} = \begin{bmatrix} \emptyset_{11} & \emptyset_{12} \\ \emptyset_{21} & \emptyset_{22} \end{bmatrix} \cdot \begin{bmatrix} \Delta_y \\ \theta_y \end{bmatrix} \quad (2)$$

where the sensitivity is defined as,

$$\emptyset_{11} = Z_{3\Delta}/\Delta_y, \ \emptyset_{12} = Z_{3\theta}/\theta_y, \ \emptyset_{21} = Z_{8\Delta}/\Delta_y \text{ and } \emptyset_{22} = Z_{8\theta}/\theta_y.$$

Note that due to the axisymmetric geometry the form of these equations and magnitudes of the sensitivities are identical for x and y oriented aberrations and misalignments as shown in the example data for M5 in Table 5.

Table 5. Tilt and coma sensitivity calculation from known perturbation in the M5 null test.

M5 Perturbation	Z_2 (µm)	Z_7 (µm)
Δ_x= 0.05 mm	-87.4668	8.7967
θ_x= .001 degree	23.23439	-2.0650
	Z_3 (µm)	Z_8 (µm)
Δ_y= 0.05 mm	-87.4668	8.7967
θ_y= .001 degree	23.2344	-2.0650

From equation (1) and equation (2) the net decenter and tilt of the mirror on the *x* and *y* axis are calculated from equation (3) and equation (4) using the Zernike coefficients from measurements,

$$\begin{bmatrix} \Delta_x \\ \theta_x \end{bmatrix} = \begin{bmatrix} \emptyset_{11} & \emptyset_{12} \\ \emptyset_{21} & \emptyset_{21} \end{bmatrix}^{-1} \cdot \begin{bmatrix} Z_2 \\ Z_7 \end{bmatrix} \quad (3)$$

$$\begin{bmatrix} \Delta_y \\ \theta_y \end{bmatrix} = \begin{bmatrix} \emptyset_{11} & \emptyset_{12} \\ \emptyset_{21} & \emptyset_{21} \end{bmatrix}^{-1} \cdot \begin{bmatrix} Z_3 \\ Z_8 \end{bmatrix} \quad (4)$$

The calculation of decenter and tilt based on measured Zernike coefficients can be used to find the absolute misalignment of the mirror within the null-test and quantify how the alignment of the mirror changes as it is rotated about an axis. The tilt and third order coma Zernike coefficients are sinusoidal with rotation angle and when the mirror optical axis is aligned with the air bearing axis the amplitude of modulation in the Zernike coefficients approaches zero.

Figure 4 shows the M5 alignment to the rotation axis of the air bearing. Data are collected every 45 degrees on rotation. The alignment of M5 to the bearing axis will be used as a representative example of the mirror alignment procedure. The average value of the Zernike coefficients represents a static misalignment of the rotation axis relative to the null-test CGH optical axis. The static misalignment is minimized to reduce measurement errors and the mirror axis is aligned to the air bearing axis by minimizing the modulation of the Zernike coefficients on rotation.

The resulting dataset for each Zernike coefficient as a function of rotation angle was given by a least-squares fit of the measurements to a sine-wave. The relative phase of the fit-functions for *x* and *y* coefficients of each aberration was set at 90 degrees and the modulation amplitudes were set equal. The amplitudes were set equal because *x* and *y* components of the same aberration must vary with the same amplitude in rotation. The 90 degree relative phase follows directly from the expectation that rotational components of *x* and *y* components of the same aberration exchange magnitudes when the optic is rotated by 90 degrees.

The sine-wave least-squares fits determine the static aberration magnitudes and orientations, rotational modulation amplitudes of the aberrations, and the orientations of the rotational components of the aberrations. The static component of all Zernike coefficients was subtracted from each fit-function in order to isolate the mirror's misalignment from the bearing axis. The mirror's position was always evaluated and adjusted at the nominal orientation. The values of the

isolated rotational components of the Zernike coefficients at the nominal orientation were entered in Equation 2 for both x and y orientations to determine the sign and magnitude of decenter and tilt of the mirror relative to the bearing. Decenter was always adjusted with two digital indicators against the OD of the mirror along the x and y axes. These indicators provided position feedback while adjusting mirror position to reduce the decenter between the mirror's optical axis and the bearing axis. Tilt was generally adjusted using the interference fringes as feedback, but the tilt of the mirror optical axis relative to the bearing was always measured during alignment of the alignment-CGH to properly quantify the resultant alignments.
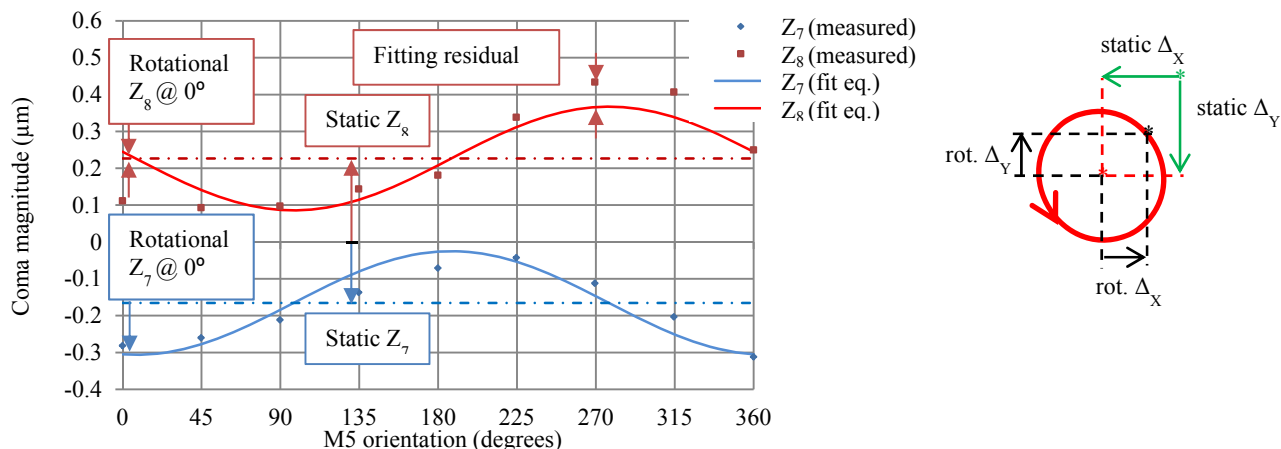
Figure 4. Example of coma data from the M5 null test with parameters relevant to the mirror alignment labeled on the plot (left) and geometric relationship of calculated axis locations (right).

2.3 Mirror alignment uncertainties

Ideally the curve-fit is representative of the mirror to bearing alignment without any mechanical instability. If the mirror deviates slightly from its ideally sinusoidal changes in position and tilt during the measurement the aberrations associated with the small deviation become residual values in the curve-fit. As the mirror approaches a level of rotational alignment that is comparable to the stability of the optical test the motion errors become dominant in the aberration data. Repeated averaged measurements at each mirror orientation ensure that the random interferometer errors are negligible in comparison to the aberration fitting residuals. Thus, the fitting residuals for aberration coefficients Z_2, Z_3, Z_7, and Z_8 at a particular orientation of the optic are correlated errors. For a given orientation the residual value of each coefficient is propagated into a mirror x direction residual using equation 1, and similarly for y using equation 2. Performing this calculation at each rotation angle generates a set of mirror position fitting residuals that are used in an RMS calculation of mirror position standard deviation for each degree of freedom. In order to claim 95% confidence in the alignment results the standard deviations of the mirror decenter and tilt are multiplied by two.

Table 6. Mirror alignment errors relative to the air-bearing axis for each CGH alignment.

	Mirror decenter magnitude (μm)	Mirror tilt magnitude (μrad)
M2, CGH1	18.5 ± 17.2	5.7 ± 5.6
M2, CGH2	13.6 ± 15.3	2.6 ± 7.2
M3, CGH1	3.7 ± 6.0	1.4 ± 2.1
M3, CGH2	3.5 ± 6.1	1.2 ± 2.2
M4, CGH1	2.4 ± 3.2	6.2 ± 12.7
M4, CGH2	2.5 ± 2.6	7.2 ± 9.7
M5, CGH1	4.1 ± 2.8	4.9 ± 3.0
M5, CGH2	4.2 ± 2.8	5.1 ± 2.9

2.4 Alignment of CGH axes to mirror axes

Runnout of the CGH center mark and changes in CGH tilt angle were observed on rotation of the mirror and minimized such that the CGH optical axis was coincident with the bearing axis. The center reference fixtures provide adjustment of the CGH position in all degrees of freedom, as shown in Figure 5. Each fixture has three steel ball-point fine threaded actuators that provide axial support near the edge of the CGH. A plastic retainer ring with three leaf-springs puts a light preload on the CGH above the axial support contacts. There are also three radial contacts separated by 120°. One contact is a passive nylon ball and spring contact. This nylon ball contact puts a preload on the CGH to hold it against two fine threaded actuators which are identical to the axial constraints. The fine threaded actuators were either picomotors or #8-100 thumb screws. With feedback from the PSM either type of actuator permits adjustment resolutions of ~1μm for decenter and ~5μrad for tilt angle. The stability of the air-bearing allowed alignment of the CGH to the bearing axis with a precision of <2 μm in centration and <5 μrad in tilt.

Leaf-spring retaining ring

Spring plunger

Axial actuators

Radial actuators

CGH
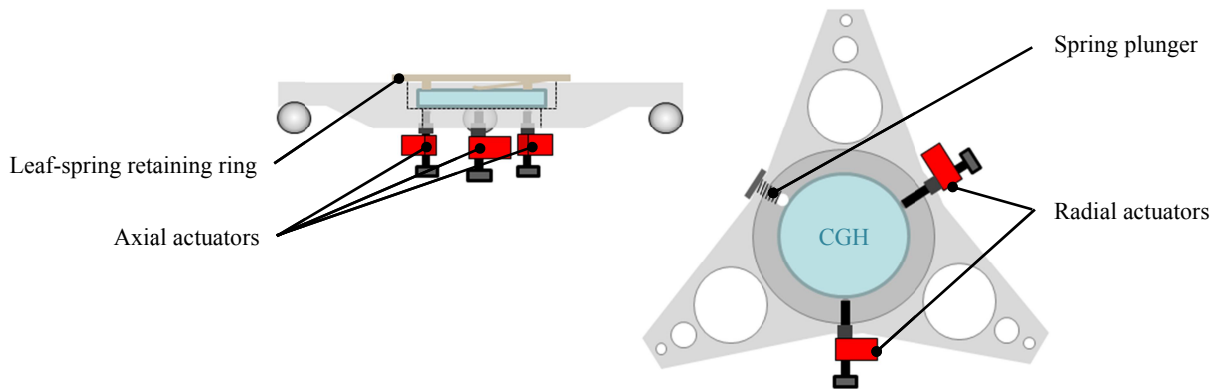
Figure 5. Geometry of actuators for CGH alignment.

The decenter and tilt of the CGH were monitored with a point source microscope (PSM) which may be used for imaging or autocollimation. In order to monitor the decenter of the CGH the PSM illuminated the surface of the CGH with a quasi-monochromatic LED and imaged a 40μm outside diameter center mark, shown in Figure 6. To monitor the CGH tilt the microscope objective was removed from the PSM and a fiber laser was used as the point source for autocollimation as in Figure 6.

270°
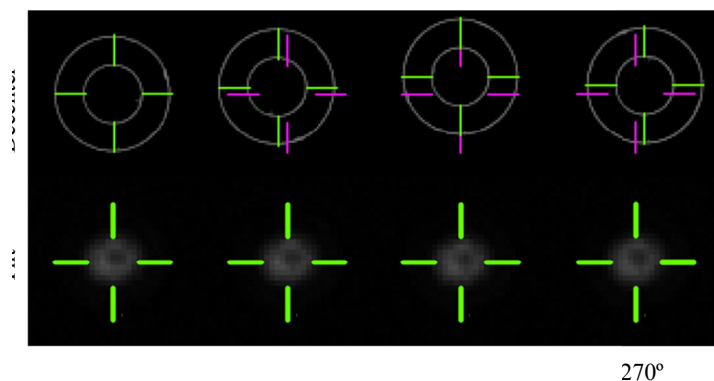
Figure 6. PSM diagnosis of the M5 CGH2 alignment after bond curing. 5.7μm residual decenter, 5μrad residual tilt.

Each CGH was bonded to the center-referencing fixture with RTV566 following the alignment procedure described above. To reduce the influence of bond contraction on the alignments the CGHs were prepared with three bond-pads to fill part of the gap from the CGH OD to the fixture ID. All of the CGHs were bonded to their fixtures with the fixtures still mounted to the mirrors. After removing the constraints each CGH was measured again to quantify its

decenter and tilt relative to the mirror axis after the bond had cured. The CGH reference alignment results, which include both measured alignment errors and uncertainties associated with the alignment diagnostics, are given in Table 7.

Table 7. CGH alignments relative to the mirrors' optical axes.

	CGH decenter magnitude (μm)	CGH tilt magnitude (μrad)
M2, CGH1	13.9 ± 24.1	10.8 ± 9.5
M2, CGH2	15.7 ± 23	5.2 ± 9.6
M3, CGH1	0.6 ± 6.0	35.9 ± 2.9
M3, CGH2	0.3 ± 6.1	21.6 ± 3.4
M4, CGH1	1.1 ± 4.5	7.6 ± 15.2
M4, CGH2	4.5 ± 4.5	8.3 ± 16.8
M5, CGH1	1.4 ± 3.8	3.6 ± 5.7
M5, CGH2	6.6 ± 4.1	5.4 ± 3.8

2.5 Registration of nested SMRs to the mirror vertex

2.6 Vertex registration of M2, M3 and M5

In order to measure the spacing between the mirrors during the system alignment there must be a reference for the vertex locations. The center reference fixtures for M2, M3 and M5 have three SMR nests so that a laser tracker can measure the reference fixture position that is registered to the vertex of the mirrors by defining the spatial relationship between the calculated mirror vertex location and the SMR nest locations.

Each mirror is aspheric and has an optical axis which passes through a center bore. Thus, there is no physical vertex for any of the mirrors in the WFC. After the as-built mirror surface parameters have been determined the mirror surface is measured with the laser tracker by holding an SMR against the optical surface in a fixture that contacts the ID of the mirror and defines a consistent radial offset to the SMR center. A set of about 20 points were measured at the ID of each mirror, followed by a set of measurements on SMRs mounted in the center reference fixtures. The measurements made in contact with the optic define a circular geometry about the mechanical axis of the mirror. The geometry of the measurements is illustrated in Figure 7.
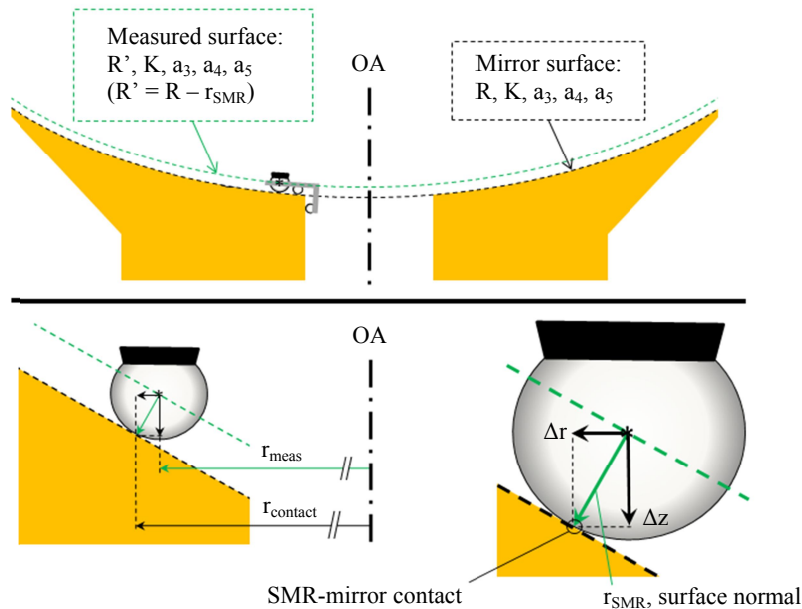
Figure 7. Cross-sectional view of the SMR in contact with the mirror. The surface subtended by the center of the SMR is shown in green and the mirror surface is in black.

Given the measured mirror parameters, the virtual surface subtended by the measurement points can be modeled as equivalent to the mirror surface with its radius of curvature reduced by the radius of the SMR.

The measured surface slope is easily determined by differentiating the sag equation and substituting the reduced radius for the mirror radius. Equation (5) and (6) give the mathematical form of the mirror surface sag and measured surface slope, respectively.

$$z(r) = \frac{r^2}{R + \sqrt{R^2 - (K+1)r^2}} + a_3 r^6 + a_4 r^8 + a_5 r^{10} \qquad (5)$$

$$z'(r) = \frac{r}{\sqrt{R'^2 - (K+1)}} + 6a_3 r^5 + 8a_4 r^7 + 10a_5 r^9 \qquad (6)$$

The circular geometry constructed through the measured points has radius r_{meas} and the slope of the measured surface at r_{meas} is used to project the appropriate radial and axial distances Δr and Δz from the measurements to the actual point of contact with the mirror surface. These offsets are applied as a change in radius and an axial location of the fit-circle to create an average region of circular contact on the optical surface.

After the circular contact of the SMR against the mirror is determined the mirror surface sag equation is used to determine the z-offset of the vertex relative to the measured points. This offset is referred to as z_{vertex}. The expressions for Δr, Δz, $r_{contact}$, and z_{vertex} are given below,

$$\Delta z = r_{SMR} \cos\left(\tan^{-1}\left(z'(r_{meas})\right)\right) \qquad (7)$$
$$\Delta r = r_{SMR} \sin\left(\tan^{-1}\left(z'(r_{meas})\right)\right) \qquad (8)$$
$$r_{contact} = r_{meas} + \Delta r \qquad (9)$$
$$z_{vertex} = -\Delta z - z(r_{contact}) \qquad (10)$$

Figure 10 shows the actual set up for the vertex registration of M2. This configuration allowed the laser tracker to be easily and stably positioned relative to the mirror and along its optical axis. In this geometry the encoder errors in the laser tracker should be symmetric and approximately equivalent between any two adjacent points.
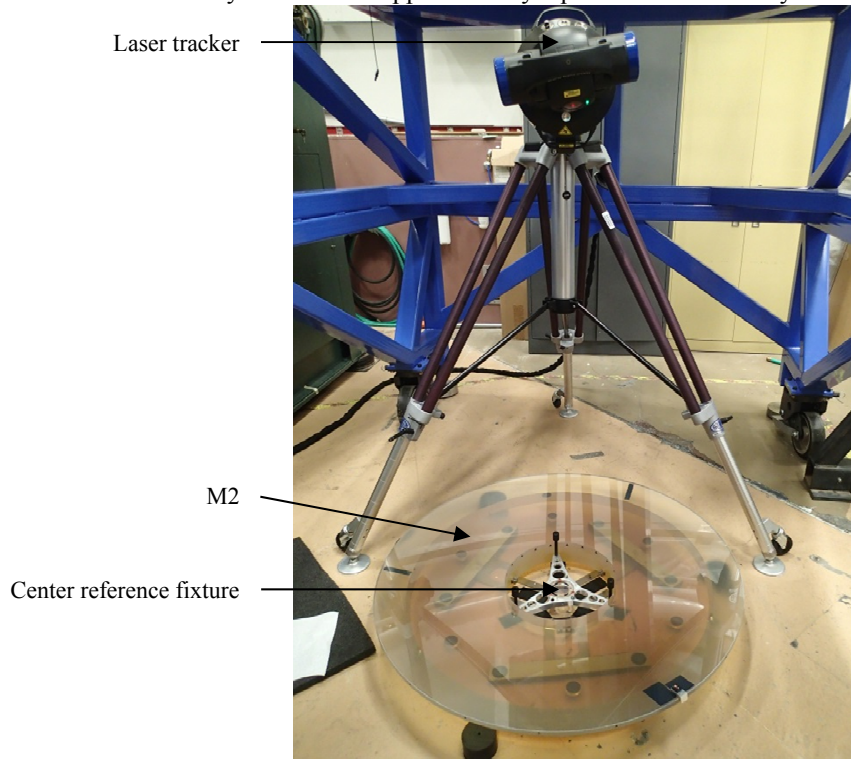
Figure 8. Laser tracker measurement setup for the M2 vertex registration. A similar configuration was also used for the M3 and M5 vertex registrations.

Table 8 presents the coordinates of the vertex of each mirror within a coordinate system that is established based on three SMR nests. The coordinate system is established by constructing a z-axis normal to a plane coincident with the

three mounted SMR centers of curvature and coincident with the centroid of the three SMR center locations. The x-axis is coincident with one particular SMR center location on each fixture. The coordinate system is established based on the locations of the SMR centers so that during the system assembly the vertex location can be constructed within the measurement set. The coordinate system is shown visually in Figure 9 using the M5 fixture as an example. The uncertainty of these coordinates includes the laser tracker measurement repeatability in measuring the mounted SMRs and determining the radius and height of the circle of measurements about the ID of the mirror. The uncertainty of the calculated vertex z-coordinate as a function of mirror surface parameter uncertainties was much smaller than the tracker uncertainties, so the glass-contact and fixture-mounted SMR measurement uncertainties dominated the vertex registration uncertainty. The independent components of the uncertainties for the M5 measurement are given in Table 8 to show how the 2σ uncertainties of the individual measurements result in the observed z-coordinate 2σ uncertainty. The uncertainty shown in Table 9 is the estimated 2σ uncertainty based on the results of several independent trials of the same vertex measurement and calculation.

Table 8. Error contributions from dataset 1 of 6 from the M5 vertex measurement.

M5 vertex-height error source	error magnitude	$2\sigma_Z$ (mm)
Mirror Radius (mm)	0.04	0.00070
Mirror Conic	0.0001	0.00001
C-fit radius (mm)	0.0032	0.0012
C-fit z-coord. (mm)	0.0036	0.0036
	RSS	**0.0039**

Table 9. Registered vertex coordinates for each mirror within the coordinate system of the SMRs.

Mirror	X (mm)	Y (mm)	Z (mm)
M2	-0.134 ± 0.009	-0.045 ± 0.014	30.326 ± 0.007
M3	0.743 ± 0.003	-0.693 ± 0.006	55.109 ± 0.008
M5	0.069 ± 0.003	-0.018 ± 0.009	-26.998 ± 0.004
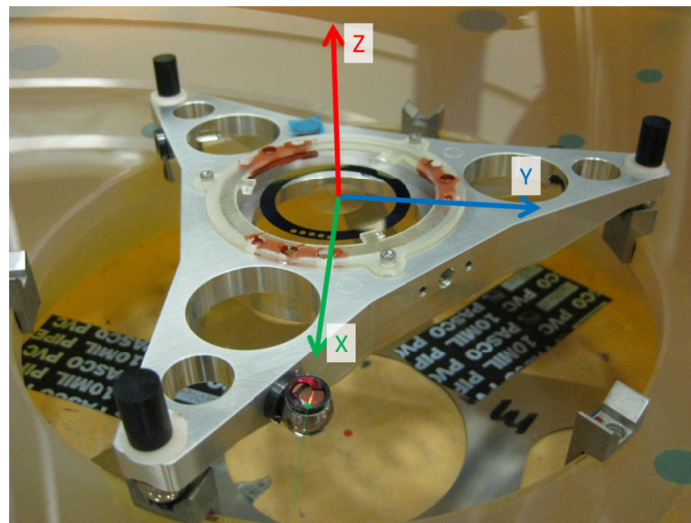
Figure 9. Reference frame defined by the center coordinates of the three SMRs on the M5 center reference fixture. Reference frame for the M2 and M3 fixtures was defined similarly.

2.7 Vertex registration of M4

The M4 vertex was registered to a single SMR on a vertex reference fixture. This was done by conducting two separate measurements. After polishing M4 its center was cored out leaving the center core undamaged. The maximum

thickness of this core was measured normal to its backplane to determine the normal distance from the polished M4 backplane to the mirror vertex. This measurement was performed by setting the planar surface of the core onto a flat and measuring both the curved surface of the core and the surface of the flat. The measurements were performed with a point source microscope attached to a coordinate measuring machine (CMM) arm, where surface points were collected by the CMM encoders as the microscope reached a cat's eye retro-reflecting condition. Figure 10 shows the core measurement setup. The points collected on the curved surface of the core were used to construct a sphere and a plane was constructed from the points measured on the surface of the flat. The maximum normal distance from the flat to the curved core surface was determined by subtracting the normal distance from the plane to the sphere's center from the radius of the sphere.

The second measurement determined the normal distance from the center of the mounted SMR to the backplane of M4. In order to determine this distance the backplane of M4 was set on top of 3 chrome steel balls on the CMM with its vertex fixture fastened to the V-blocks, as shown in Figure 11. The CMM was used again with a point source microscope in order to measure the center of curvature location and radius of each ball contacting the M4 backplane and of the SMR mounted in the fixture. This measurement was performed 4 times and both M4 and its fixture were re-mounted each time the measurement was conducted.
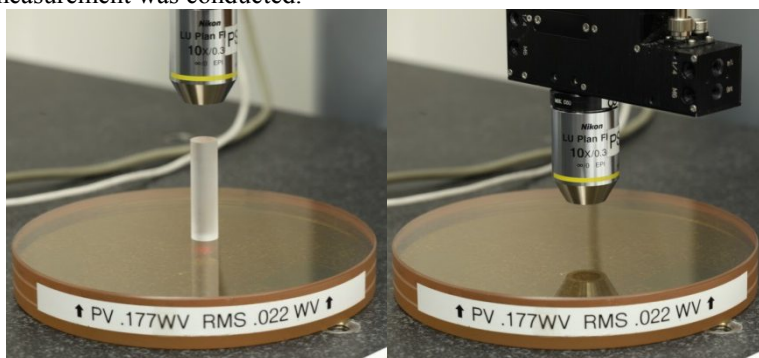
Figure 10. PSM on a CMM arm measuring the curved surface of the M4 core (left), and measuring the flat underneath the core (right).
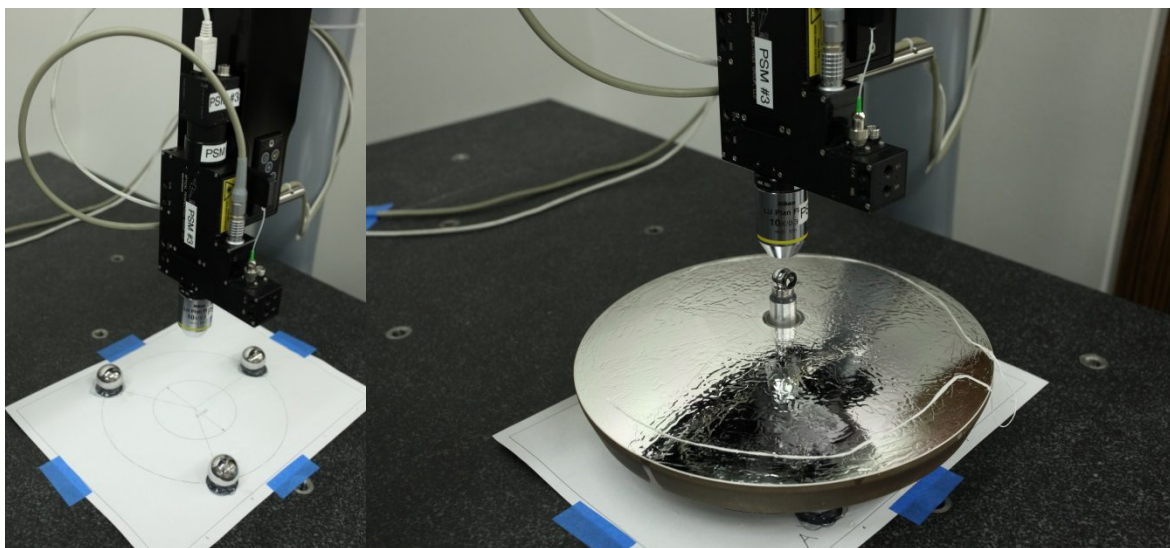
Figure 11. PSM on a CMM arm measuring the radii and center positions of the M4 support which is three steel balls (left) and the center of an SMR mounted in the M4 vertex reference fixture (right).

After conducting the measurements the data was processed in Spatial Analyzer. The data sets were transformed to match each other to best-fit, where the locations of the three balls contacting the backplane were aligned to each other at center of curvature. A total of 14 measurements were collected, per ball, to determine their radii. A reference frame was constructed such that the xy plane was coincident with the mirror backplane by ensuring that the center of curvature of each ball had a z-offset from the plane equal to its measured radius. The z-coordinates of the measured SMR locations in

this reference frame were used to determine the expected offset of the SMR from the M4 backplane along its surface normal. The SMR location was registered to the vertex location by calculating the difference between the core thickness and the SMR offset from the M4 backplane. The measured quantities and their individual uncertainties are summarized in Table 10 to show how the final result was found.

Table 8. Uncertainties contributing to the M4 vertex reference fixture registration uncertainty.

Quantity	Value (mm)	Uncertainty, 2σ
Core surface radius	359.9213	0.00057
Core center of curvature to backplane	316.1135	0.00053
Ball A radius	12.703	0.0014
Ball B radius	12.304	0.0010
Ball C radius	12.699	0.0010
SMR center height from backplane	70.0568	0.0064
SMR to vertex, normal distance	**26.2490**	**0.0066**

3. INITIAL ALIGNMENT OF THE WIDE FIELD CORRECTOR WITH A LASER TRACKER

A reference frame was established based on the locations of three hemispherical kinematic mounting interfaces on the corrector's frame to meet the system requirement for the location of the optical axis of the WFC in the telescope. This reference frame is illustrated in Figure 12. Within this reference coordinate frame the mirrors have prescribed nominal z- coordinates that are derived from the system prescription in Table 1. The CGH in each mounted center reference fixture must be aligned such that it is centered on and normal to the z-axis.
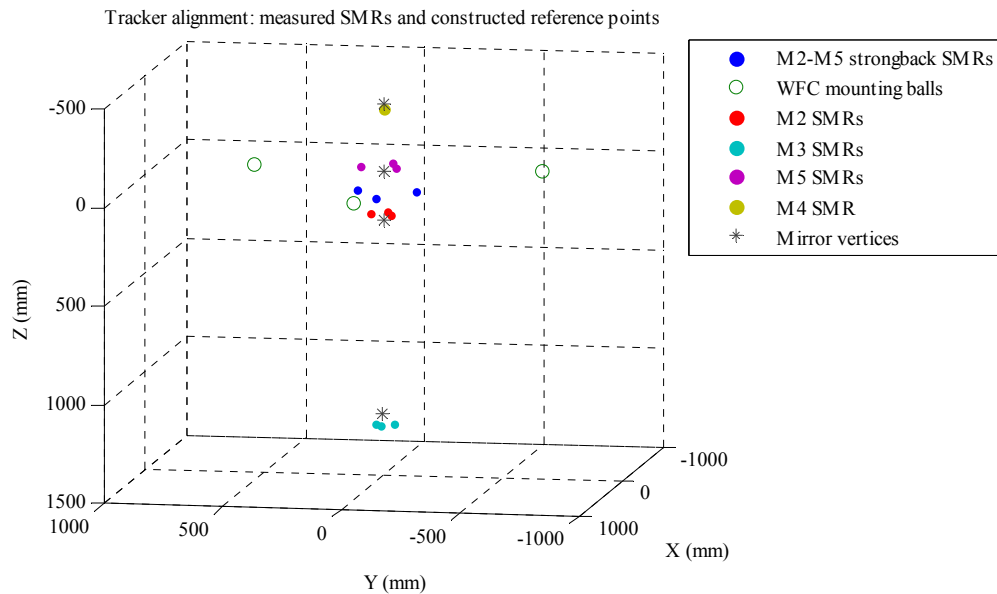
Figure 12. Reference frame for the WFC system alignment.

Although the laser tracker only serves as a final alignment reference for mirror spacing it is very useful for initial mirror alignment. The three SMR locations on the center reference fixtures for M2, M3, and M5 were registered to the centroid and plane of their reference CGHs using the PSM mounted on a CMM arm, as shown in Figure 13. This registration allows the set of mounted SMR locations for each fixture to be used as a reasonably accurate reference from which to define mirror tilt and centration. After this registration is performed the mirror's reference locations are diagnosed within the reference frame of the corrector to determine how the mirror must be moved to achieve its nominal alignment.
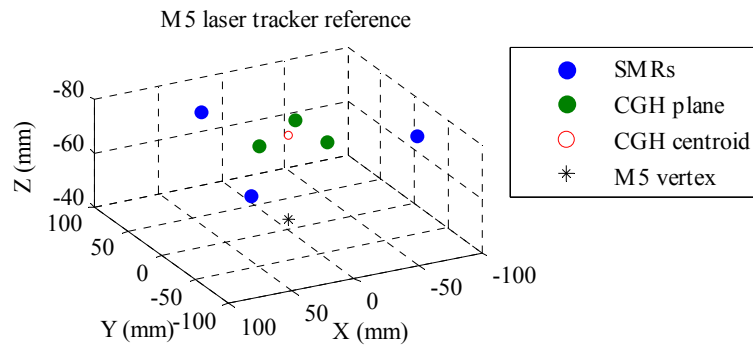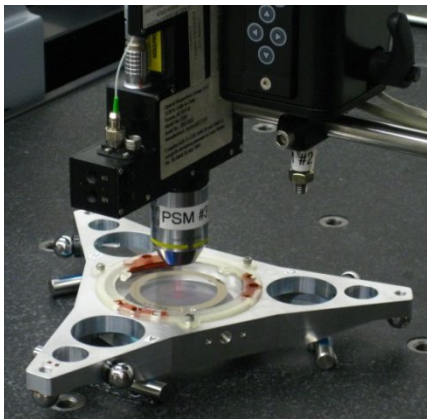
Figure 13. M5 center reference fixture in measurement setup under the PSM on a CMM (left) and measured points of SMR centers, points on the plane of the CGH, location of the CGH centroid, and registered vertex location (right).

With the guidance of the laser tracker the wide field corrector is aligned to the specification of initial alignment as in Table 11.

Table 11. initial mirror alignment error using the center reference fixtures with the laser tracker guidance

	M2	M3	M4	M5
Tilt, X (µrad)	-23	-5	N/A	13
Tilt, Y (µrad)	23	-24	N/A	-4
Decenter, X (µm)	6	-15	13	26
Decenter, Y (µm)	9	16	-1	-38
Axial position error, Z (µm)	-69	-9	-8	4

4. CONCLUDING REMARK

A previous testing of the proposed alignment scheme with the center reference fixtures was able to provide alignment diagnostic errors as small as 3 µm in decenter and 6 µrad in tilt [3]. The laser tracker is expected to introduce less than 5 µm of axial spacing uncertainty during the final alignment. The levels of uncertainty and residual errors achieved in the reference alignments and much smaller errors expected during their use in alignment provides confidence in the successful alignment of the Wide Field Corrector.

Currently the wide field corrector is aligned to the specification for initial alignment by the guidance of laser tracker. The next planned stage is to align the mirrors in the Wide Field Corrector using an autocollimator and video microscope in conjunction with the CGHs in the center reference fixtures. Finally, the alignment of Wide Field Corrector will be verified by system wavefront tests using CGHs and an interferometer to test the full system as well as isolated paris of mirrors.

REFERENCES

[1] Gary J. Hill, John A. Booth, Mark E. Cornell, et al, "Current status of the Hobby Eberly Telescope wide field upgrade," Proc. of SPIE Vol. 8444, (2012)
[2] James H. Burge, S. Benjamin, M. Dubin, A. Manuel, M. Novak, C. J. Oh, M. Valente, C. Zhao, "Development of a wide field spherical aberration corrector for the Hobby Eberly Telescope," Proc. of SPIE Vol. 7733, (2010)
[3] L.E. Coyle, M. Dubin, J.H. Burge, "Low uncertainty alignment procedure using computer generated holograms," Proc. of SPIE Vol. 8131, (2011)